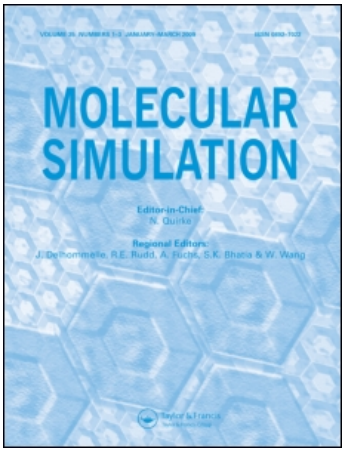

Molecular Simulation

Publication details, including instructions for authors and subscription information:
http://www.informaworld.com/smpp/title~content=t713644482

A DFT study of the effect of K and SiO_2 on syngas conversion to methane and methanol over an Mo_6P_3 cluster

Sharif F. Zaman[a]; Kevin J. Smith[a]

[a] Department of Chemical and Biological Engineering, University of British Columbia, Vancouver, BC, Canada

First published on: 02 September 2009

To cite this Article Zaman, Sharif F. and Smith, Kevin J.(2010) 'A DFT study of the effect of K and SiO_2 on syngas conversion to methane and methanol over an Mo_6P_3 cluster', Molecular Simulation, 36: 2, 118 — 126, First published on: 02 September 2009 (iFirst)

To link to this Article: DOI: 10.1080/08927020903124585

URL: http://dx.doi.org/10.1080/08927020903124585

Molecular Simulation
Vol. 36, No. 2, February 2010, 118–126

Taylor & Francis
Taylor & Francis Group

A DFT study of the effect of K and SiO_2 on syngas conversion to methane and methanol over an Mo_6P_3 cluster

Sharif F. Zaman and Kevin J. Smith*

Department of Chemical and Biological Engineering, University of British Columbia, 2360 East Mall, Vancouver, BC, Canada V6T 1Z3

(*Received 31 March 2009; final version received 17 June 2009*)

Synthesis gas ($CO + H_2$) conversion to CH_4 and CH_3OH over an Mo_6P_3 cluster, an $Mo_6P_3-Si_3O_9$ and a $K-Mo_6P_3-Si_3O_9$ cluster has been studied using density functional theory (DFT). The study focused on the reaction between the intermediate species $CH_2OH_{ad} + H_{ad}$, comparing methanol formation to C—O bond scission that yields $CH_{2.ad} + H_2O_{ad}$ species. The activation energies of both the reactions decreased on the $Mo_6P_3-Si_3O_9$ and the $K-Mo_6P_3-Si_3O_9$ clusters compared to the Mo_6P_3 cluster. However, on the $K-Mo_6P_3-Si_3O_9$ cluster, the activation energy for methanol formation (12.1 kcal/mol) was higher than the C—O bond-breaking activation energy (9.9 kcal/mol). Although the DFT study predicted preferential formation of CH_4 versus CH_3OH on all the Mo_6P_3 clusters, the study also predicted an increased formation of CH_3OH with the addition of K and experimental measurements are in agreement with this prediction.

Keywords: MoP; catalyst; reaction; syngas; carbon monoxide; hydrogen; methanol; methane; cluster model; $DMol^3$; DFT

1. Introduction

Modern theoretical chemistry can be used to understand chemical reactivity and mechanisms of heterogeneous catalytic reactions [1–4]. Density functional theory (DFT) can be employed to calculate the formation energy of molecules and solids with high accuracy and information related to the surface reaction can also be determined. Computational chemistry can be used as a tool for catalyst design by calculating the catalyst's suitability for a particular reaction, without experimentation. Thus, a computational approach towards understanding the role of different catalyst components in a particular reaction is available and this principle has been reported in the literature [5,6]. Promoters also play a key role in heterogeneous catalysis, their use being necessary in many successful industrial catalysts. A simple tool for modifying the surface properties of catalytic materials, widely exploited in heterogeneous catalysis, consists of alkali metal doping [7], the alkali metal acting as an electronic promoter. The dopant enhances the catalytic properties of the active phase, due to its ability to modify the chemisorption properties of the catalyst surface and to affect the chemisorptive bond strength of reactants and reaction intermediates. The most pronounced electronic promotion has been found in the case of K, Rb and Cs. Many of the promotional effects of K are characteristic of the other alkali metals [8].

Researchers have used computational chemistry to investigate the influence of alkali metal (K) on transition metals (Pt, Ru, Rh and Fe) to understand the dissociative adsorption of CO and N_2 relevant to the Fischer–Tropsch and ammonia synthesis, respectively [8,9]. Liu and Hu [10] also used DFT to investigate surface structural effects on C—O bond dissociation, and reported that surface kinks facilitate bond scission.

For the methanol synthesis, CO must adsorb non-dissociatively [11–14] on the active site before being hydrogenated to produce the stable formyl (CHO) surface species [15] that leads to the formation of methanol or higher alcohols. Rh-based catalysts are known to be effective for syngas conversion to alcohols [16,17] and they give high selectivity to ethanol (44.5 C atom%) when promoted with Mn [18]. Recent research has focused on Mo-based catalysts (i.e. MoS_2, Mo_2C, Mo_2N and MoP), as they have the characteristics of precious metals (Pt and Rh) [19]. Recently, Pistonesi et al. [20] have reported methanol adsorption and dissociation to methoxy on an Mo_2C surface. No reports on the use of DFT to study the effect of alkali promoter on syngas conversion over Mo catalysts are available, although Kotarba et al. [21] have reported on the modification of the surface electronic properties of Mo_2C as a function of K loading.

The microkinetic network of syngas ($CO + H_2$) conversion to methane and methanol over an Mo_6P_3 cluster, used to simulate an MoP catalyst, was reported previously [22]. An adsorbed hydroxymethyl (CH_2OH_{ad}) species was shown to be a common intermediate for both CH_4 and CH_3OH formation. In the present paper, cluster models of $Mo_6P_3-Si_3O_9$ and $K-Mo_6P_3-Si_3O_9$ were built and used to investigate the hydrogenation of the CH_2OH_{ad}

*Corresponding author. Email: kjs@interchange.ubc.ca

ISSN 0892-7022 print/ISSN 1029-0435 online

DOI: 10.1080/08927020903124585
http://www.informaworld.com

species to yield methanol, as well as the C—O bond scission of CH_2OH_{ad} to yield surface $CH_{2.ad}$ and H_2O_{ad} species. Results from this study provide insight into the effects of K on MoP catalyst selectivity in syngas conversion reactions.

2. Methods

The DMol^3 module of Materials Studio (version 4.0) from Accelrys, Inc. (San Diego, CA, USA) was used to complete the DFT calculations [23]. Accordingly, the electronic wave functions are expanded in numerical atomic basis sets defined on an atomic-centred spherical-polar mesh. The double-numerical plus *d*-function (DND) all electron basis set was used for all the calculations. The DND basis set includes one numerical function for each occupied atomic orbital and a second set of functions for valence atomic orbitals, plus a polarisation *d*-function on all non-hydrogen atoms. The Becke exchange [24] plus Perdew–Wang approximation [25] non-local functional (GGA-PW91) was used in all the calculations. Each basis function was restricted to a cut-off radius of 4.7 Å, allowing for efficient calculations without loss of accuracy. The Kohn–Sham equations [26] were solved by a self-consistent field procedure. The techniques of direct inversion in an iterative subspace (DIIS) [27] with a size value of 6 and thermal smearing of 0.005 Ha [28] were applied to accelerate convergence. The optimisation convergence thresholds for energy change, maximum force and maximum displacement between the optimisation cycles were 0.00002 Ha, 0.004 Ha and 0.005 Å, respectively. The activation energy between two surface species was identified by complete linear synchronous transit and quadratic synchronous transit search methods [29], followed by transition state (TS) confirmation through the nudge elastic band method [30]. Spin polarisation and symmetry were imposed in all the calculations.

In the present work, a cluster model of the MoP catalyst surface has been used. A cluster model is an incomplete representation of the electronic properties of a catalyst surface because of its small size and discrete nature. But it enables rigorous quantum mechanical calculation to elucidate the extent of orbital overlap and electronic correlation of the adsorbate surface ensemble. This allows one to predict the adsorption geometry, adsorption energy and surface reactivity with less expense in computational power compared to a complete surface model. In the present study, we have investigated the reaction steps on three cluster models.

The MoP cluster models and the reactant and product species were created using the Material Studio Visualizer. The adsorption energy was calculated by subtracting the energies of the gas phase species and the cluster from the energy of the adsorbed species according to the equation: $E_{ad} = E_{(adsorbate/cluster)} - (E_{adsorbate} + E_{cluster})$. With this definition, a negative E_{ad} corresponds to a stable surface species. The activation energy was calculated by using the TS search tool in DMol^3, applied to the reactant, a stable surface species plus an adsorbed H atom (H_{ad}) on the clusters, and the product.

3. Results

3.1 Building the Mo_6P_3 clusters

The procedure for building a cluster model of MoP was described in detail elsewhere [22]. Accordingly, we have built the same Mo_6P_3 cluster as a model of the (100) surface of MoP in this study, as illustrated in Figure 1.

A cluster model of SiO_2 was incorporated into the Mo_6P_3 cluster to simulate the effect of support properties on MoP/SiO_2 catalysts. The SiO_2 support can be modelled in different molecular arrangements, described by the number of Si atoms in the SiO_2 ring. Molecules with three, five, seven and nine Si atoms have been proposed [31], and in the present work, a three Si atom ring cluster with three oxygen atoms in the ring and another six oxygen atoms attached to Si atoms as dangling bonds was used. The angles and bond lengths between Si and O in the cluster ring are given in Table 1. The SiO_2 cluster model is in good agreement with that described by the West and Hench [31] model.

The procedure used to construct the cluster of the present study is depicted in Figure 1. The Mo_6P_3 cluster was placed on the Si_3O_9 cluster and the total arrangement was geometrically optimised to determine the Mo_6P_3–Si_3O_9 cluster structure. Since the Mo_6P_3 cluster has three different faces, three different arrangements of the Mo_6P_3 on the Si_3O_9 cluster were investigated and the minimum energy configuration was used in further analysis. A K atom was then introduced on one side of the Mo_6P_3–Si_3O_9 cluster and two different sites of Mo were investigated on this cluster. Site I, designated as Mo_I, had the Mo atom closest to the K atom. The influence of K would be expected to be significant at this site whereas, on the Mo atom far from the K atom – site II, designated as Mo_{II} – the influence would be small. The adsorption of the reaction intermediates on each of the Mo sites, bound through the C and O atoms of the intermediates, was each investigated separately as part of the study.

The electronic charge on the Mo and the K for the Mo_6P_3–Si_3O_9 and K–Mo_6P_3–Si_3O_9 clusters is listed in Table 2. Introduction of the K atom imposed a negative charge ($-0.263e$) on the Mo_I atom, whereas Mo_{II} contained a positive charge of $0.118e$. In comparison, on the Mo_6P_3–Si_3O_9 cluster, both the Mo_I and Mo_{II} atoms possessed a positive charge of 0.160 and $0.145e$, respectively.

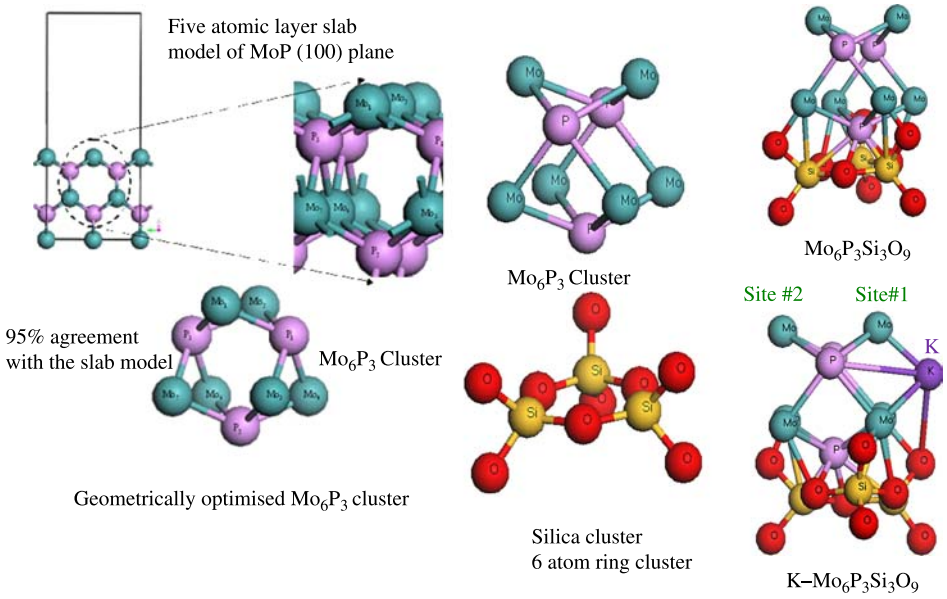

Figure 1. Cluster models of Mo_6P_3, $Mo_6P_3Si_3O_9$ and K–$Mo_6P_3Si_3O_9$.

Table 1. Threefold SiO_2 cluster model structure.

r_{Si-O} (Å)	$r_{O\bar{o}O}$ (Å)	$r_{Si\bar{o}Si}$ (Å)	Θ_{O-Si-O} (deg)	$\Theta_{Si-O-Si}$ (deg)	Ref.
1.62	2.52	2.96	102.00	132.00	[31]
1.65	2.65	3.02	107.12	132.85	This work

Table 2. Atomic charge distribution on the Mo_6P_3–Si_3O_9 and K–Mo_6P_3–Si_3O_9 cluster.

	Mo_I	Mo_{II}	K	O	C
Mo_6P_3					
Empty cluster	0.60	0.60	–	–	–
$CH_2OH_{ad} + H_{ad}$	0.25	0.22	–	−0.66	−0.47
CH_3OH_{ad}	0.14	0.04	–	−0.67	−0.39
Mo_6P_3–Si_3O_9					
Empty cluster	0.16	0.15	–	–	–
$CH_2OH_{ad} + H_{ad}$	0.34	0.23	–	−0.67	−0.49
CH_3OH_{ad}	0.21	0.13	–	−0.71	−0.39
K–Mo_6P_3–Si_3O_9					
Empty cluster	−0.26	0.12	0.89	–	–
CH_2OH_{ad}[a] + H_{ad}	−0.77	0.28	0.93	−0.53	−0.65
CH_3OH_{ad}[a]	−0.17	0.08	0.86	−0.41	−0.67

[a]O atom adsorbed on site I of the K–Mo_6P_3–Si_3O_9 cluster.

3.2 *Reactions on the Mo_6P_3 clusters*

3.2.1 *C—O bond cleavage*

The C—O bond cleavage of CH_2OH_{ad} was initiated with a hydroxymethyl species and a hydrogen atom adsorbed on the cluster. The products were adsorbed methyl ($CH_{2.ad}$) and water species. A comparison of this reaction step on the three different clusters is depicted in Figures 2(a), 3(a) and 4(a),(b). Relevant structural data are summarised in Table 3.

Figure 2(a) shows that the hydroxymethyl species was adsorbed on the Mo_6P_3 cluster through a bridge bond, with the C atom bound to one Mo atom and the O atom bound to the other Mo atom. For Mo_6P_3 (Figure 2(a)) and K–Mo_6P_3–Si_3O_9 site II (Figure 4(b)), the H atom was adsorbed on the Mo atom where the O atom of the CH_2OH_{ad} species was bound. On the Mo_6P_3–Si_3O_9 (Figure 3(a)) and the K–Mo_6P_3–Si_3O_9 site I (Figure 4(a)), the H was bound on a different Mo atom. The molecular arrangement of the reactants facilitates the C—O bond-breaking step on the cluster. The results (Table 3) show that the C—Mo and O—Mo bond lengths decreased with the addition of SiO_2 and K to the Mo_6P_3 cluster, implying that the CH_2OH_{ad} species was more tightly bound on the clusters with Si_3O_9 and K, and this observation was supported by the increased adsorption energy of the hydroxymethyl species on the Mo_6P_3–Si_3O_9 and K–Mo_6P_3–Si_3O_9 sites I and II, compared to the Mo_6P_3 cluster (Table 3).

After breaking the C—O bond of the CH_2OH_{ads} species, the surface species $CH_{2.ad} + H_2O_{ad}$ were generated on the Mo_6P_3, Mo_6P_3–Si_3O_9 and K–Mo_6P_3–Si_3O_9 site I clusters, and $CH_{2.ad} + HO_{ad} + H_{ad}$ species were formed on site II of the K–Mo_6P_3–Si_3O_9 cluster. The adsorption energy of $CH_{2.ad} + H_2O_{ad}$ on the Mo_6P_3, Mo_6P_3–Si_3O_9 and K–Mo_6P_3–Si_3O_9 site I clusters was −145.97, −145.51 and −154.27 kcal/mol, respectively. On site II of the K–Mo_6P_3–Si_3O_9 cluster, $CH_{2.ad} + OH_{ad} + H_{ad}$ species had an adsorption energy of −156.35 kcal/mol. The adsorption energies increased on the Mo_6P_3–Si_3O_9 and K–Mo_6P_3–Si_3O_9 clusters compared to Mo_6P_3. The highest adsorption energy was observed on the

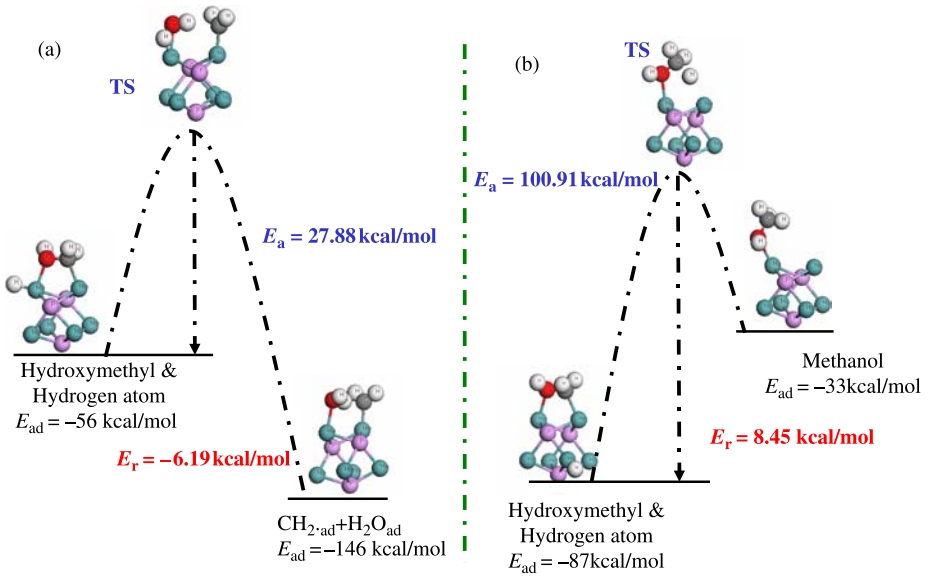

Figure 2. (a) C—O dissociation of CH_2OH_{ad} species over Mo_6P_3 cluster; (b) methanol formation from CH_2OH_{ad} species over Mo_6P_3 cluster.

K-doped cluster, implying greater stability of the adsorbed species on the K-doped cluster than the un-doped Mo_3P_6–Si_3O_9 cluster. C—Mo bond lengths on the Mo_6P_3, Mo_6P_3–Si_3O_9 and K–Mo_6P_3–Si_3O_9 sites I and II were 1.96, 1.92, 2.17 and 2.12 Å, respectively. Compared to Mo_6P_3, the C—Mo bond length decreased on the Mo_6P_3–Si_3O_9 but increased on the K-doped Mo_6P_3–Si_3O_9 cluster. On both the Mo_6P_3–Si_3O_9 and K–Mo_6P_3–Si_3O_9 clusters, the $CH_{2.ad}$ species formed a geminal structure (the carbon atom was attached to two different Mo atoms as shown in Figure 4(a)), and this resulted in an increase in adsorption energy compared to the other two structures. The geminal carbon of the $CH_{2.ad}$ species and the strong binding energies on the K-doped catalysts may promote either the insertion of CO_{ad} species to produce higher oxygenates or the homologation of $CH_{2.ad}$ species to produce higher hydrocarbons.

The O—Mo atomic distance for H_2O_{ad} species on the Mo_6P_3, Mo_6P_3–Si_3O_9 and K–Mo_6P_3–Si_3O_9 (site I) species was 2.23, 2.31 and 3.35 Å, respectively. The distance increased with Si_3O_9 and K addition to the

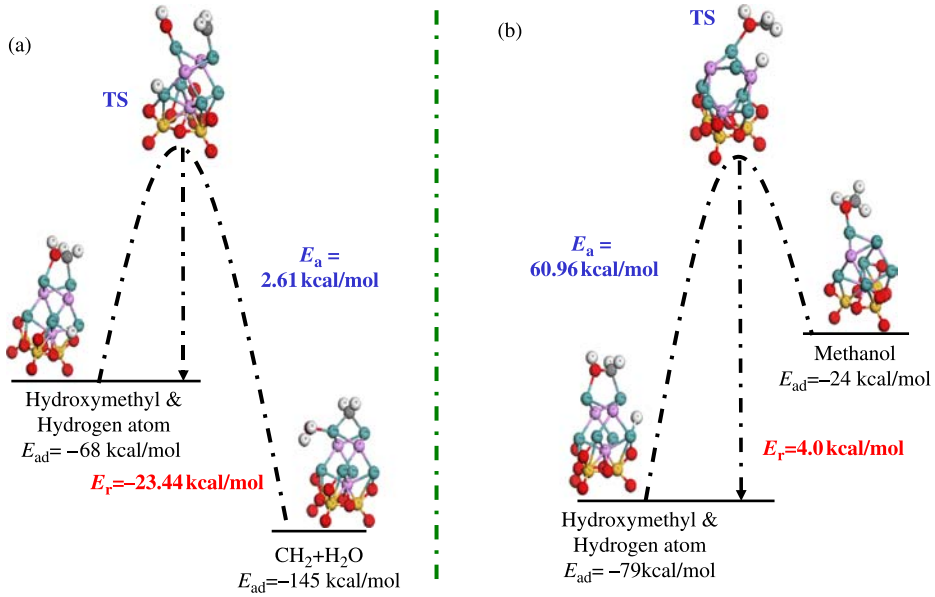

Figure 3. (a) C—O dissociation of CH_2OH_{ad} species over Mo_6P_3–Si_3O_9 cluster; (b) methanol formation from CH_2OH_{ad} species over Mo_6P_3–Si_3O_9 cluster.

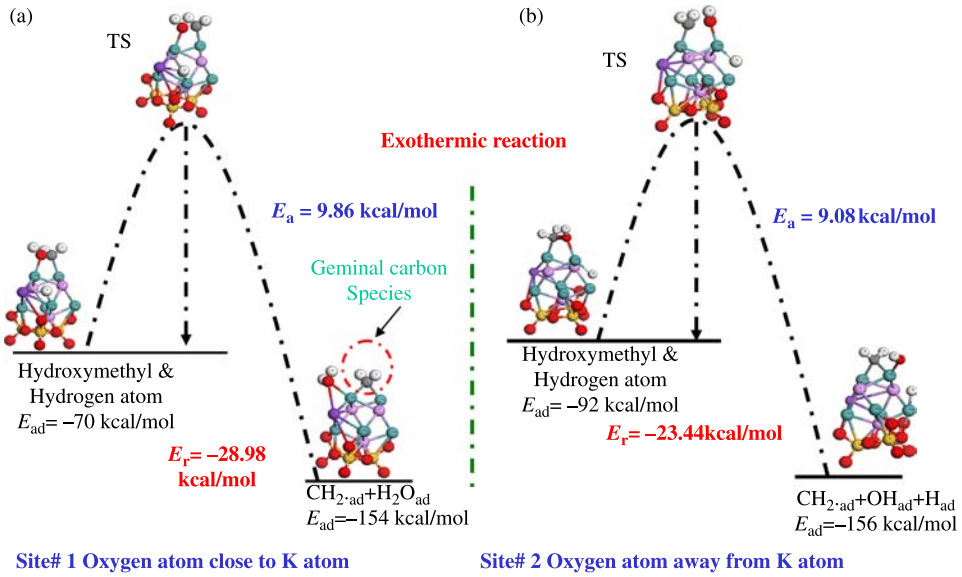

Figure 4. C—O dissociation of CH_2OH_{ad} species over K–Mo_6P_3–Si_3O_9 cluster: (a) O atom adsorbed on Mo atom close to K atom; (b) C atom adsorbed on Mo atom close to K atom.

Table 3. Reactant and product bond length, bond angle and adsorption energy for C—O bond scission step.

	Bond length			Bond angle			
Cluster models	O–Mo_I (Å)	C–Mo_{II} (Å)	C–O (Å)	∠C–Mo_{II}–Mo_I (deg)	∠O–Mo_I–Mo_{II} (deg)	∠C–O–Mo_I (deg)	Adsorption energy ΔE (kcal/mol)
CH_2OH_{ad} + H_{ad}							
Mo_6P_3	2.28	2.20	1.49	69.17	66.46	–	− 54.88
Mo_6P_3–Si_3O_9	2.26	2.18	1.49	68.52	66.68	111.64	− 68.49
Site I. K–Mo_6P_3–Si_3O_9	2.20	2.15	1.51	65.96	68.62	113.74	− 70.56
Site II. K–Mo_6P_3–Si_3O_9[a]	2.18[b]	2.14[c]	1.48	63.72[d]	69.94[e]	105.27[f]	− 92.47
$CH_{2.ad}$ + H_2O_{ad}							
Mo_6P_3	2.23	1.96	–	97.60	79.28	–	− 145.97
Mo_6P_3–Si_3O_9	2.31	1.92	–	91.31	125.32	–	− 145.51
Site I. K–Mo_6P_3–Si_3O_9	2.35	2.17	–	43.62	135.90	–	− 154.27
Site II. K–Mo_6P_3–Si_3O_9[a]	2.93[b]	2.12[c]	–	43.47[d]	144.70[e]	–	− 156.35

[a] $CH_{2.ad}$ + $OH_{.ad}$ + $H_{.ad}$ species on site II.
[b] O–Mo_{II}.
[c] C–Mo_1.
[d] ∠C–Mo_I–Mo_{II}.
[e] ∠O–Mo_{II}–Mo_I.
[f] ∠C–O–Mo_{II}.

Mo_6P_3, indicating that H_2O will form readily on the K-doped MoP. For the OH species adsorbed on site II of the K–Mo_6P_3–Si_3O_9 cluster, the O—Mo distance was 2.93 Å.

The TS structure information for the hydroxymethyl reaction step over the Mo_6P_3, Mo_6P_3–Si_3O_9 and the K–Mo_6P_3–Si_3O_9 sites I and II clusters is reported in Table 5. Enthalpies of reaction were calculated as − 6.19, − 23.44, − 28.98 and − 23.44 kcal/mol for the Mo_6P_3, Mo_6P_3–Si_3O_9 and K–Mo_6P_3–Si_3O_9 sites I and II clusters, respectively. As the bond-breaking reaction is highly exothermic, very high negative values for the heat of reaction were observed for this step. Comparing the activation energies, the value calculated on the Mo_6P_3 cluster (27.88 kcal/mol) decreased to 2.61 kcal/mol on the Mo_6P_3–Si_3O_9 cluster, whereas on the K–Mo_6P_3–Si_3O_9 cluster the values were 9.85 and 9.08 kcal/mol for sites I and II, respectively.

3.2.2 *Methanol formation*

Methanol formation was modelled by H_{ad} attached to different Mo sites close to the C atom of the CH_2OH_{ad} species as the reactant, with the formation of CH_3OH_{ad} as the product. The CH_3OH_{ad} species was adsorbed via the O atom on a Mo site of the clusters. The reaction step for the Mo_6P_3, Mo_6P_3–Si_3O_9 and K–Mo_6P_3–Si_3O_9 sites I and II

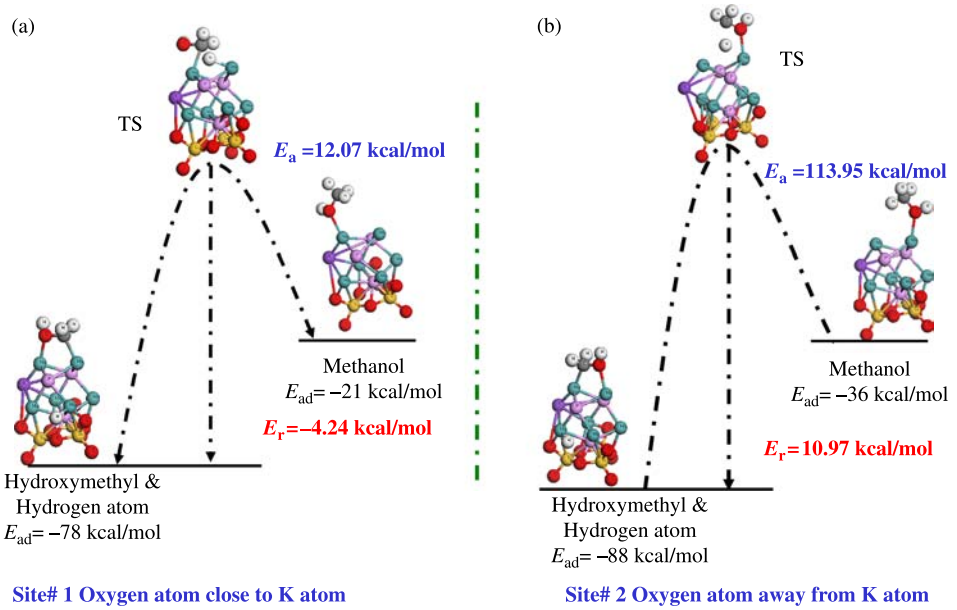

Figure 5. Methanol formation from CH_2OH_{ad} species over K–Mo_6P_3–Si_3O_9 cluster: (a) O atom adsorbed on Mo atom close to K atom; (b) C atom adsorbed on Mo atom close to K atom.

Table 4. Reactant and product bond length, bond angle and adsorption energy for methanol formation.

	Bond distance			Bond angle			
Cluster models	O–Mo_I (Å)	C–Mo_{II} (Å)	C–O (Å)	∠C–Mo_{II}–Mo_I (deg)	∠O–Mo_I–Mo_{II} (deg)	∠C–O–Mo_I (deg)	Adsorption energy, ΔE (kcal/mol)
CH_2OH_{ad} + H_{ad}							
Mo_6P_3	2.23	2.21	1.48	67.70	67.03	–	−86.94
Mo_6P_3–Si_3O_9	2.24	2.189	1.50	66.08	69.17	113.85	−78.86
Site I. K–Mo_6P_3–Si_3O_9	2.20	2.15	1.51	65.96	68.62	113.74	−78.86
Site II. K–Mo_6P_3–Si_3O_9	2.19[a]	2.16[b]	1.48	62.31[c]	71.01[d]	102.58[e]	−88.32
CH_3OH_{ad}							
Mo_6P_3	2.32	–	1.45	–	110.03	–	−33.21
Mo_6P_3–Si_3O_9	2.24	–	1.46	–	146.03	125.69	−23.75
Site I. K–Mo_6P_3–Si_3O_9	2.28	–	1.46	–	113.16	119.71	−20.75
Site II. K–Mo_6P_3–Si_3O_9	2.23[a]	–	1.46	–	105.07[d]	128.84[e]	−35.74

[a] O–Mo_{II}.
[b] C–Mo_I.
[c] ∠C–Mo_I–Mo_{II}.
[d] ∠O–Mo_{II}–Mo_I.
[e] ∠C–O–Mo_{II}.

is depicted in Figures 2(b), 3(b), 5(a),(b) and the bond information of each surface species is reported in Table 4.

Data for the reactant structure, reported in Table 4, show that the adsorption energy decreased on the Mo_6P_3–Si_3O_9 and K–Mo_6P_3–Si_3O_9 clusters (O atom adsorbed at site I) but increased on the K–Mo_6P_3–Si_3O_9 cluster (O atom adsorbed at site II), compared to the Mo_6P_3 cluster. The O—Mo bond length decreased with the addition of K and the same trend was observed for the C—Mo bond length. The distances between C—O were similar on all the clusters.

The CH_3OH_{ad} species was adsorbed on all the clusters via the O atom. The O—Mo distances and the C—O bond lengths are reported in Table 4. The adsorption energy of CH_3OH_{ad} on the Mo_6P_3, Mo_6P_3–Si_3O_9 and K–Mo_6P_3–Si_3O_9 sites I and II clusters was −33.21, −23.75, −20.75 and −35.74 kcal/mol, respectively. The lowest adsorption energy was observed on the K–Mo_6P_3–Si_3O_9 cluster at site I (O adsorbed close to the K atom), but the adsorption energy was much higher than that reported on other methanol producing catalysts such as Cu(111) −4.38 kcal/mol [32], Pd(111) −6.46 kcal/mol [33], Pt(111) −7.61 kcal/mol [34] and Ni(111) −0.46 kcal/mol [35]. Recently, Pistonesi et al. [20] have reported an adsorption energy of −8.97 kcal/mol for methanol on a Mo_2C cluster. Since the Mo_6P_3 clusters of the present study show much higher adsorption energy for

Table 5. Transition state for the reaction steps, C—O bond scission and methanol formation from CH_2OH_{ad}.

Cluster models	O–Mo_1 (Å)	C–Mo_{II} (Å)	C–O (Å)	∠C–Mo_{II}–Mo_I (deg)	∠O–Mo_I–Mo_{II} (deg)	∠C–O–Mo_I (deg)	E_a (kcal/mol)	E_r (kcal/mol)
$CH_2OH_{ad} + H_{ad} \rightarrow$ $CH_{2.ad} + H_2O_{ad}$								
Mo_6P_3	1.80	1.99	–	94.31	76.84	–	27.88	−6.19
Mo_6P_3–Si_3O_9	1.96	1.973	–	67.82	107.53	–	2.61	−23.44
Site I. K–Mo_6P_3–Si_3O_9	2.21	1.93	–	65.83	101.71	–	9.86	−28.98
Site II. K–Mo_6P_3–Si_3O_9[a]	2.02[b]	2.11[c]	–	62.25[d]	75.65[e]	–	9.08	−23.44
$CH_2OH_{ad} + H_{ad} \rightarrow$ CH_3OH_{ad}								
Mo_6P_3	2.30	2.28	1.52	–	73.94	–	100.91	8.45
Mo_6P_3–Si_3O_9	2.22	–	1.41	–	103.82	111.73	60.96	4.00
Site I. K–Mo_6P_3–Si_3O_9	2.11	–	1.44	–	76.98	–	12.07	−4.24
Site II. K–Mo_6P_3–Si_3O_9	2.20[b]	–	1.47	–	92.48[e]	118.29[f]	113.95	10.97

[a] $CH_{2.ad} + OH_{ad} + H_{ad}$ species on site II.
[b] O–Mo_{II}.
[c] C–Mo_1.
[d] ∠C–Mo_I–Mo_{II}.
[e] ∠O–Mo_{II}–Mo_I.
[f] ∠C–O–Mo_{II}.

methanol than these metals, there is a likelihood that on MoP catalysts, strongly adsorbed CH_3OH may be available for further reaction and C-addition to yield C_{2+} products.

Figures 2(b), 3(b), 5(a),(b) depict the $CH_2OH_{ad} + H_{ad} \rightarrow CH_3OH_{ad}$ reaction step over the Mo_6P_3, Mo_6P_3–Si_3O_9 and the K–Mo_6P_3–Si_3O_9 sites I and II clusters. The TS structure information is summarised in Table 5. Activation energies for this reaction step were 100.91, 60.96, 12.07 and 113.95 kcal/mol and the enthalpies of the reaction were 8.45, 4.00, −4.24 and 10.97 kcal/mol on the Mo_6P_3, Mo_6P_3–Si_3O_9 and K–Mo_6P_3–Si_3O_9 sites I and II clusters, respectively. The lowest activation energy was for site I of the K–Mo_6P_3–Si_3O_9 cluster. The activation energy decreased by a factor of five compared to the Mo_6P_3–Si_3O_9 cluster and by a factor of eight compared to the Mo_6P_3 cluster. Enthalpies of reaction were positive (endothermic) except for the configuration where the O atom was adsorbed on site I of the K–Mo_6P_3–Si_3O_9 cluster, which had a TS configuration that gave rise to an exothermic value.

4. Discussion

The charge distribution on the C and O atoms of the CH_3OH_{ad} and $CH_2OH_{ad} + H_{ad}$ species, adsorbed on the Mo_6P_3, Mo_6P_3–Si_3O_9 and K–Mo_6P_3–Si_3O_9 clusters, is reported in Table 2. The C atom of the free CH_3OH had positive charge of $0.062e$ and the O atom had negative charge of $-0.502e$. However, the adsorbed C and O atoms had negative charges for all the cases investigated herein. For the Mo_6P_3 and Mo_6P_3–Si_3O_9 clusters, the O had more negative charge than the C and the magnitude of the charges on the atoms did not vary significantly over each of the two clusters. For the K–Mo_6P_3–Si_3O_9 cluster, the C atom showed a more negative charge than the O atom. In this case, electron donation from K to the Mo_I followed by electron transfer to the O occurred. Hence, charge was shifted to the C atom to compensate for the surface bond between Mo_I and O. The negative charge on the Mo_I atom of the K–Mo_6P_3–Si_3O_9 site I cluster decreased the adsorption energy of CH_3OH (20.75 kcal/mol) compared to the Mo_6P_3, Mo_6P_3–Si_3O_9 clusters because of the repulsion of negative charges.

A decrease in the activation energy of the methanol formation step was observed on the Mo_6P_3–Si_3O_9 cluster compared to the Mo_6P_3 cluster. The activation energy was 100.91 kcal/mol for the Mo_6P_3 cluster and 60.96 kcal/mol for the Mo_6P_3–Si_3O_9 cluster. Similarly, the activation energy of the C—O scission reaction step decreased from 27.88 to 2.61 kcal/mol. With the addition of K, the activation energy for CH_3OH_{ad} formation was significantly decreased to 12.07 kcal/mol on site I of the K–Mo_6P_3–Si_3O_9 cluster. For site II, a higher activation energy of 113.95 kcal/mol was observed. On the other hand, for the C—O bond-breaking step, the activation energy increased to 9.85 and 9.08 kcal/mol for the K–Mo_6P_3–Si_3O_9 sites I and II, respectively. Clearly, these results show that the C—O bond scission of the CH_2OH_{ad} species is favoured over CH_3OH_{ad} species formation over all of the Mo_6P_3 clusters investigated.

The authors recently reported on the activity of 10 wt% MoP on SiO_2 catalysts, promoted with 1 and 5 wt% K [36]. The catalyst activity was determined in a laboratory fixed bed microreactor under reaction conditions of 275°C, 8.2 MPa and a gas-hourly space velocity (GHSV) of $3600\,h^{-1}$. The catalysts were operated at these conditions for an average of at least 50 h time-on-stream. For the 10 wt% MoP on SiO_2 catalyst, a high selectivity to methane

(35.2 C atom%) was measured. With increased K doping, selectivity to CH_4 decreased to 22.1 and 9.0 C atom% over the 1 and 5 wt% K-doped $MoP-SiO_2$ catalyst, respectively. Methanol selectivity was low in all cases with values of 0.6, 2.2 and 0.3 C atom% measured over the $MoP-SiO_2$ catalysts, the 1 wt% $K-MoP-SiO_2$ and the 5 wt% $K-MoP-SiO_2$, respectively. For the 1 wt% K-doped catalysts, an increase in methanol selectivity and a decrease in methane selectivity were observed, whereas for the 5 wt% K-doped catalyst, both the selectivity to methanol and methane decreased, relative to the MoP catalyst. High selectivity towards C_{2+} oxygenates, especially ethanol, acetaldehyde and acetone, was also observed with increased K loading. Low selectivity to methanol over the 5 wt% K-doped catalyst suggested the conversion of methanol to other products, i.e. ethanol and acetone. The DFT model presented herein is in agreement with these experimental findings. Both the model and the experimental data show that methane is produced selectively over MoP and increased methanol selectivity was observed for the K-doped cluster and catalyst. The high adsorption energy of methanol over MoP clusters suggests that methanol will undergo further surface reaction to produce higher alcohols and/or other oxygenates, as observed on the K promoted MoP catalysts.

5. Conclusions

The DFT calculations on model Mo_6P_3 clusters showed that the addition of K decreased the activation energy for the formation of methanol on site I of the $K-Mo_6P_3-Si_3O_9$ cluster to 12.07 kcal/mol, whereas the activation energy for the C—O bond cleavage reaction was lower (9.88 kcal/mol). Hence, the model calculations predicted that addition of K would enhance methanol production on MoP catalysts, although CH_4 would dominate the product compared to methanol, in agreement with experimental data reported over K-doped MoP catalysts supported on SiO_2.

Acknowledgement

Financial support from the Natural Sciences and Engineering Research Council (NSERC) of Canada is gratefully acknowledged.

References

[1] P.S. Bagus, A. Clotet, D. Curulla, F. Illas, and J.M. Ricart, *Charge displacement analysis: A new general method to estimate atomic charges in molecules and clusters*, J. Mol. Catal. A: Chem. 119 (1997), pp. 3–10.

[2] M. Neurock, *Chapter 8: catalysis in application of molecular and material modeling*, in *Applications of Molecular and Materials Modeling*, International Technology Research Institute, Baltimore, MD, 2002, pp. 77–105.

[3] K. Morokuma, *Chapter 2: Electronic structure, thermochemistry and kinetics*, in *Applications of Molecular and Materials Modeling*, International Technology Research Institute, Baltimore, MD, 2002, pp. 7–16.

[4] X. Krokidis, J.W. Andzelm, N. Govind, and V. Milman, *Quantum technology in catalysis*, Appl. Catal. A Gen. 280 (2005), pp. 105–113.

[5] C.J.H. Jacobsen, S. Dahl, B.S. Clausen, S. Bahn, A. Logadottir, and J.K. Norskov, *Catalyst design by interpolation in the periodic table: Bimetallic ammonia synthesis catalysts*, J. Am. Chem. Soc. 123 (2001), pp. 8404–8405.

[6] M. Kubo, T. Kubota, C. Jung, M. Ando, S. Sakahara, and K. Yajima, *Design of new catalysts for ecological high-quality transportation fuels by combinatorial computational chemistry and tight-binding quantum chemical molecular dynamics approaches*, Catal. Today 89 (2004), pp. 479–493.

[7] C.G. Vayenas, S. Brosda, and C. Pliangos, *Rules and mathematical modeling of electrochemical and chemical promotion: 1. Reaction classification and promotional rules*, J. Catal. 203 (2001), pp. 329–350.

[8] R. Schlögl, *Alkali metals in heterogeneous catalysis*, in *Physics and chemistry of alkali metal adsorption*, H. P. Bonzel, A. M. Bradshaw and G. Ertl, eds., Elsevier, Amsterdam, 1989, pp. 347–375.

[9] W.D. Mross, *Alkali doping in heterogeneous catalysis*, Catal. Rev. 25 (1983), pp. 591–637.

[10] Z. Liu and P. Hu, *General rules for predicting where a catalytic reaction should occur on metal surfaces: a density functional theory study of C—H and C—O bond breaking/making on flat, stepped, and kinked metal surfaces*, J. Am. Chem. Soc. 125 (2003), pp. 1958–1967.

[11] R.A. Sheldon (ed.), *Chemicals from Synthesis Gas. Catalytic Reactions of CO and H_2*, Springer, Berlin, 1983, 216 p.

[12] K.J. Smith, R.G. Herman, and K. Klier, *Kinetic modeling of higher alcohol synthesis over alkali-promoted Cu/ZnO and MoS_2 catalysts*, Chem. Eng. Sci. 45 (1990), pp. 2639–2646.

[13] P. Chaumette, Ph. Courty, A. Kiennemann, and B. Ernst, *Higher alcohol and paraffin synthesis on cobalt based catalysts: Comparison of mechanistic aspects*, Top. Catal. 2 (1995), pp. 117–126.

[14] K. Klier, R.G. Herman, J.G. Nunan, K.J. Smith, C.E. Bogdan, and C. Young, *Mechanism of methanol and higher oxygenate synthesis*, in *Studies in Surface Science and Catalysis*, D. M. Bibby, C. D. Chang, R. F. Howe and S. Yurchak, eds., Elsevier, Amsterdam, 1988, pp. 109–125.

[15] J.G. Nunan, C.E. Bogdan, K. Klier, K.J. Smith, C. Young, and R.G. Herman, *Higher alcohol and oxygenate synthesis over cesium-doped Cu/ZnO catalysts*, J. Catal. 116 (1989), pp. 195–221.

[16] J.P. Hindermann, G.J. Hutchings, and A. Kiennemann, *Mechanistic aspects of the formation of hydrocarbons and alcohols from carbon monoxide hydrogenation*, Catal. Rev. Sci. Eng. 35 (1993), pp. 1–127.

[17] P.C. Ellgen, W.J. Bartley, M.M. Bhasin, and T.P. Wilson, *Rhodium-based catalysts for the conversion of synthesis gas to two-carbon chemicals*, Adv. Chem. 178 (1979), pp. 147–157.

[18] J. Hu, Y. Wang, C. Cao, D.C. Elliott, D.J. Stevens, and J.F. White, *Conversion of biomass-derived syngas to alcohols and C_2 oxygenates using supported Rh catalysts in a microchannel reactor*, Catal. Today 120 (2007), pp. 90–95.

[19] S.T. Oyama, *Novel catalysts for advanced hydroprocessing: Transition metal phosphides*, J. Catal. 216 (2003), pp. 343–352.

[20] C. Pistonesi, A. Juan, A.P. Farkas, and F. Solymosi, *DFT study of methanol adsorption and dissociation on β-$Mo_2C(0\ 0\ 1)$*, Surf. Sci. 602 (2008), pp. 2206–2211.

[21] A. Kotarba, G. Adamski, W. Piskorz, Z. Sojka, C. Sayag, and G. Djega-Mariadassou, *Modification of electronic properties of Mo_2C catalyst by potassium doping: Impact on the reactivity in hydrodenitrogenation reaction of indole*, J. Phys. Chem. B 108 (2004), pp. 2885–2892.

[22] S.F. Zaman and K.J. Smith, *A study of synthesis gas conversion to methane and methanol over a Mo_6P_3 cluster using density functional theory*, Mol. Simul. 34 (2008), pp. 1073–1084.

[23] B. Delley, *From molecules to solids with the DMol^3 approach*, J. Chem. Phys. 133 (2000), pp. 7756–7764.
[24] A.D. Becke, *A multicenter numerical integration scheme for polyatomic molecules*, J. Chem. Phys. 88 (1988), pp. 2547–2553.
[25] J.P. Perdew and Y. Wang, *Accurate and simple analytic representation of the electron-gas correlation energy*, Phys. Rev. B 45 (1992), pp. 13244–13249.
[26] W. Kohn and L.J. Sham, *Self-consistent equations including exchange and correlation effects*, Phys. Rev. A 140 (1965), pp. 1133–1138.
[27] P. Pulay, *Improved SCF convergence acceleration*, J. Comp. Chem. 3 (1982), pp. 556–560.
[28] B. Delley, J. M. Seminorio & P. Politzer, (eds.), *Modern Density Functional Theory: A Tool for Chemistry (Theoretical and Computational Chemistry)*, Elsevier Science, Amsterdam, 1995.
[29] S. Bell and J.S. Crighton, *Locating transition states*, J. Chem. Phys. 80 (1984), pp. 2464–2475.
[30] G. Henkelman and H. Jonsson, *Improved tangent estimate in the nudged elastic band method for finding minimum energy paths and saddle points*, J. Chem. Phys. 113 (2000), pp. 9978–9985.
[31] J.K. West and L.L. Hench, *Molecular orbital of silica rings and their vibrational spectra*, J. Am. Ceram. Soc. 74 (1995), pp. 1093–1096.
[32] J. Greeley and M. Mavrikakis, *Methanol decomposition on Cu(111): A DFT study*, J. Catal. 208 (2002), pp. 291–300.
[33] M. Neurock, *First-principles analysis of the hydrogenation of carbon monoxide over palladium*, Top. Catal. 9 (1999), pp. 135–152.
[34] S. Kandoi, J. Greeley, A.M. Sanchez-Castillo, S.T. Evans, A.A. Gokhale, J.A. Dumesic, and M. Mavrikakis, *Prediction of experimental methanol decomposition rates on platinum from first principles*, Top. Catal. 37 (2006), pp. 17–28.
[35] I.N. Remediakis, F. Abild-Pedersen, and J.K. Norskov, *DFT study of formaldehyde and methanol synthesis from CO and H_2 on Ni(111)*, J. Phys. Chem. B 108 (2004), pp. 14535–14540.
[36] S.F. Zaman and K.J. Smith, *Synthesis gas conversion over MoP catalysts*, Catal. Commun. 10 (2009), pp. 468–471.